Dynamics of Populations of Planetary Systems
Proceedings IAU Colloquium No. 197, 2005
Z. Knežević and A. Milani, eds.

DOI: 10.1017/S1743921304008786

Nongravitational Accelerations on Comets

Steven R. Chesley[1] and Donald K. Yeomans
Jet Propulsion Laboratory, M/S 301-150, Pasadena, CA 91109, USA
[1]email: Steven.R.Chesley@jpl.nasa.gov

Abstract.
The orbital motion of comets is difficult to characterize accurately due to the rocket-like outgassing of material from the cometary nucleus. The resulting nongravitational accelerations often appear to be fundamentally stochastic in nature and thus pose severe modeling challenges in orbit determination, especially when the comet has been observed for many revolutions. Even so, new techniques have arisen in recent years that give new insight, not only into the motion of the comets, but also into their physical characteristics and spin states. These approaches include modeling of spin axis precession over many decades and the consideration of the seasonal variation in the thrust from discrete jets acting on a rotating nucleus. Such advances have been enabled, in part, by the increasing efforts and capabilities of comet observers worldwide as more and more comets with longer and longer observing arcs become available for study. In this review we specifically consider the application of the Rotating Jet Model to several space mission targets, indicating how this model can often be used to infer the orientation of a comet's spin axis.

Keywords. Comets, orbit determination, nongravitational accelerations

1. Introduction

A detailed historical introduction to the nongravitational accelerations affecting the motions of comets has recently been provided by Yeomans *et al.* (2004a), and so here we will provide only a short introduction to this topic for completeness.

Even though it was only the second comet predicted to return to perihelion, Comet 2P/Encke exhibited anomalous orbital behavior already at its first predicted return in 1822, behavior that was inconsistent with a trajectory governed solely by the gravitational influences of the sun and planets. It was Encke himself who noted that his eponymous comet arrived at perihelion a few hours earlier than his predictions. He proposed an interplanetary resisting medium to explain the phenomenon (Encke 1823), a medium that he envisaged as an extension of the solar atmosphere or the remains of cometary and planetary atmospheres. This model allowed Encke to accurately predict the perihelion passages of his comet between 1825 and 1858. Variations on Encke's resisting model were utilized for much of the nineteenth century but in the first half of the twentieth century, problems arose when the motions of comets 14P/Wolf and 6P/d'Arrest were consistent with an increasing, rather than a decreasing, orbital period (Kamieński 1933, Recht 1940). Clearly a mechanism was required whereby orbital energy could be added to, as well as subtracted from, a comet's orbital motion.

While little recognized at the time, Bessel (1836) had pointed out that a comet expelling material in a radial sunward direction would suffer a recoil acceleration, and if the expulsion of material took place asymmetrically with respect to perihelion, there would be a decrease or increase in the comet's orbital period depending upon whether the comet expelled more material before or after perihelion. Although Bessel did not identify the expulsion of material with the vaporization of ices, his basic concept of cometary

nongravitational accelerations would ultimately prove to be correct. The development of Whipple's (1950, 1951) icy conglomerate model for the cometary nucleus finally put the rocket-like effect of an outgassing cometary nucleus on a firm physical footing and laid the ground work for more sophisticated models that could account for the cometary nongravitational accelerations. The so-called standard model for cometary nongravitational accelerations, which has the comet's outgassing reaching a peak at perihelion, was introduced by Marsden *et al.* (1973). A modification of this model by Yeomans & Chodas (1989) allowed the comet's outgassing to peak on either side of perihelion. Since these two models will be discussed in some detail in Sec. 2, we will move on to summarize some alternate nongravitational acceleration models that have been employed to represent the long-term motion of active periodic comets.

Partly to account for the time dependence found for some cometary nongravitational effects, Whipple & Sekanina (1979) and Sekanina (1981, 1984) introduced a linear precession model for a spherically symmetric nucleus. In this case, the outgassing acceleration does not act upon the nucleus center-of-mass and hence a torque is introduced causing the nucleus spin axis to precess with time. This introduces a time-varying nongravitational effect from apparition to apparition in a natural manner. Within this model, Sitarski (1995, 1996) introduced a time shift that allowed the outgassing peak to be reached before or after perihelion. Sekanina's (1984) forced precession model for the cometary nucleus, where he derived formulae for changes of the spin-axis orientation, was extended by Królikowska *et al.* (1998) for a nonspherical nucleus. In models of this type, solutions are made for the corrections to the six orbital elements and several additional parameters that include the obliquity of the nucleus, the magnitude of the nongravitational acceleration at one AU and the three angles that describe the direction of the nongravitational acceleration vector in orbital coordinates.

More recently, a Rotating Jet Model (RJM) has been introduced to model discrete outgassing jets on the surface of a cometary nucleus. That is, the nongravitational thrusting acting upon the nucleus takes place only when these active surface areas are exposed to sunlight and this depends upon the orientation of the nucleus spin pole. In a series of papers, Sekanina (1988a, 1988b, 1993) discussed the rotating jet model and used it to interpret the observed sunward fan-like coma of Comet 2P/Encke as an effect of northern and southern localized jets upon the surface of this comet's nucleus. The rotation averaged orbital components of the nongravitational acceleration for a nucleus with active jets was adapted for orbital computations by Szutowicz (2000) and independently by Chesley (2002). This model is described further in Sec. 3, and used to model the motions of several comets in Sec. 4.

2. The Extended Standard Model

The notion that comet nongravitational accelerations were caused by sublimating ices eventually led to the development of a model that proved effective in describing the variation of outgassing activity with heliocentric distance. That model, introduced by Marsden *et al.* (1973), is explicitly given by

$$\mathbf{a} = g(r)\,(A_1\,\hat{\mathbf{e}}_R + A_2\,\hat{\mathbf{e}}_T + A_3\,\hat{\mathbf{e}}_N). \tag{2.1}$$

Here the so-called $g(r)$ function reflects the sublimation rate of water ice as a function of heliocentric distance; $g(r)$ decays roughly as r^{-2} out to around 2 AU, and then much more steeply ($\sim r^{-23.5}$) beyond about 3 AU where the sublimation of water ice is substantially halted. This function remains a central feature of virtually all nongravitational acceleration models, even as these models have become increasingly complex.

https://doi.org/10.1017/S1743921304008786 Published online by Cambridge University Press

The A_i in Eq. 2.1 are constant parameters that give the nongravitational acceleration the comet would experience when it is at 1 AU in each of the three coordinate directions. The accelerations are referred to the classical heliocentric Radial-Transverse-Normal (RTN) reference frame, denoted by $\hat{\mathbf{e}}_R$, $\hat{\mathbf{e}}_T$ and $\hat{\mathbf{e}}_N$, respectively. Marsden *et al.* (1973) reported that it was generally sufficient to neglect out-of-plane accelerations, and so, since its introduction, this model has been usually restricted to in-plane accelerations, i.e., $A_3 = 0$. However, the majority of the comets that we have investigated as a part of potential or actual flight mission studies have revealed substantial out-of-plane accelerations, and so, while the practice of neglecting A_3 has become commonplace, we have found that this practice is often not well-founded.

The standard formulation places the peak acceleration at the point of perihelion passage, while there are numerous comets known to exhibit marked asymmetries with respect to perihelion in their outgassing activity. To model this effect, Yeomans & Chodas (1989) applied a time offset ΔT to $g(r)$, essentially shifting the peak outgassing activity some number of days before or after perihelion. In other words, they replaced $g(r)$ by $g(r')$, where $r' = r(t') = r(t + \Delta T)$. In doing so Yeomans & Chodas found markedly improved orbital fits and predictions for a few comets, most notably 6P/d'Arrest, and moderate improvements for several other comets. Interestingly, they reported little improvement for two comets, 67P/Churyumov-Gerasimenko and 26P/Grigg-Skjellerup, that were known to exhibit notable perihelion asymmetries in their brightness.

Combining the foregoing formulations, we obtain the Extended Standard Model (ESM), a four-parameter (A_1, A_2, A_3 and ΔT) model that is the most versatile model available. Its utility lies in its simplicity. There is no requirement for *a priori* knowledge of the comet's physical characteristics or spin state, and no allowance for the possibility that nongravitational effects could vary from revolution to revolution. The success of this approach is due to the fact that most comets do not behave erratically over intervals up to a few orbital periods. Thus it works remarkably well across a wide cross-section of comets and it can be applied with a minimum of preliminary analysis. Still, the model assumes uniform behavior from revolution to revolution and does not specifically model more complex factors such as seasonal fluctuations in outgassing activity. For these, more refined approaches are necessary.

3. Rotating Jet Model

The *instantaneous* acceleration of a cometary jet depends upon the intrinsic jet strength A_J, the heliocentric distance r and the solar zenith angle z at the jet source according to

$$\mathbf{a}_J = -A_J\, g(r) \cos z\, \hat{\mathbf{e}}_J \tag{3.1}$$

when $z \geqslant 0$. For $z < 0$, i.e., when the source is in darkness, we have $\mathbf{a}_J = 0$. Here $\hat{\mathbf{e}}_J$ denotes the unit vector of the instantaneous jet direction. This formulation allows one to interpret A_J as a normalized acceleration; it is the magnitude of the acceleration when the sun is at the jet's zenith and the comet is at 1 AU from the sun.

As explained in detail in Appendix A, the *mean* acceleration of a cometary jet, averaged over a single comet rotation, is given by

$$\bar{\mathbf{a}}_J = g(r) A_J\, (J_S\, \hat{\mathbf{e}}_S + J_P\, \hat{\mathbf{e}}_P), \tag{3.2}$$

where the unit vector $\hat{\mathbf{e}}_P$ denotes the direction of the rotation axis and the unit vector $\hat{\mathbf{e}}_S$ denotes the most sunward direction in the the comet's equatorial plane. (The averaging is independent of the rotation direction, and so $\hat{\mathbf{e}}_P$ could refer to either the north or

https://doi.org/10.1017/S1743921304008786 Published online by Cambridge University Press

south pole.) The parameters J_S and J_P account for the daily insolation experienced by the particular jet, assuming a spherical figure. They depend upon the "season" (subsolar latitude) and the thrust angle η that the jet forms with the rotation pole (i.e., the jet's colatitude). When the jet is in the polar night regime $J_S = J_P = 0$ and there is no acceleration. The equations for J_S and J_P in the diurnal and polar day regimes are given in Appendix A, which also describes an extension to account for diurnal lag in the jet's activity.

The RJM is particularly attractive because it is a much higher fidelity model of a comet's outgassing activity than the ESM. Moreover, multiple jets can easily be accounted for by superposition. The RJM fully accounts for the fact that at various points along the orbit some source regions are continually shutdown during polar night, others are continually active during polar day, and still others are active only part of the day during the diurnal regime. This varying activity leads to nongravitational accelerations that may not be well modeled by the ESM. Further, with the RJM approach, only certain pole orientations can produce the observed accelerations, which allows the spin axis to be estimated in some cases. Of course, one problem is that some *a priori* knowledge of the comet's spin axis and the location of jets is generally required. However, as we show below, even without this information, the RJM can be used with considerable success to derive these quantities.

4. Application to selected actual or potential space mission targets

We investigate the nongravitational accelerations acting on several selected space mission targets: past, present and future. The six selected comets and the respective observational data sets that we have used are detailed in Table 1. These comets (and their associated space missions) include, 19P/Borrelly (Deep Space 1), 81P/Wild 2 (Stardust), 9P/Tempel 1 (Deep Impact), 67P/Churyumov-Gerasimenko (Rosetta), along with 2P/Encke and 6P/d'Arrest (erstwhile targets of the ill-fated CONTOUR mission).

In Table 2 we list for each comet the best-fitting values for the ESM parameters, along with their formal uncertainties. Here the formal uncertainties are most useful to judge the statistical significance of a result, rather than as an indication of the true value of the parameter, since in some cases the values can vary significantly from apparition to apparition. We also list in Table 2 the pole that can be inferred from the estimated ESM parameters according to the technique described below for Borrelly. Finally, the table includes the normalized (i.e., dimensionless) Root Mean Square (RMS) of the fit.

Table 3 lists the best-fitting RJM parameters. In every case we have assumed two jets, one acting on each hemisphere, with fixed thrust angles. When jet locations are known from other sources we use the published values, otherwise we use a generic configuration with one near-polar jet on the northern hemisphere ($\eta = 10°$) and a mid-latitude jet on the southern hemisphere ($\eta = 135°$). Although the thrust angles were not varied, a systematic search for the best-fitting pole direction was conducted by exploring a 5°-raster in the R.A.-Dec. space of possible pole orientations. The best-fitting pole thus obtained is tabulated for each case, along with the associated jet strengths and the normalized RMS. In all of the RJM fits, we actually fit only the comet orbital elements and the jet strengths A_{J_i}; the thrust angles and pole orientations were held fixed during the fits.

4.1. *Comet 19P/Borrelly*

Comet 19P/Borrelly was the target of a September 2001 flyby of NASA's Deep Space 1 spacecraft. About two weeks before the encounter, the spacecraft imaged the comet and

https://doi.org/10.1017/S1743921304008786 Published online by Cambridge University Press

Table 1. Comet Observational Data Used in Fits

	No. Obs.	First Obs.	Last Obs.	No. App.
19P/Borrelly	1671	1980-Jul-21.3	2002-Jun-11.9	4
81P/Wild 2	1853	1988-Sep-09.5	2003-Dec-30.9	3
2P/Encke	1538	1989-Jun-01.6	2004-Jul-17.4	5
6P/d'Arrest	387	1982-Apr-23.3	2001-May-25.3	4
9P/Tempel 1	706	1967-Jun-08.4	2003-Dec-26.9	8
67P/C.-G.	1005	1988-Jul-06.4	2004-Jun-20.0	3

Table 2. Results for Extended Standard Model

	$A_1 \times 10^{10}$ (AU/d^2)	$A_2 \times 10^{10}$ (AU/d^2)	$A_3 \times 10^{10}$ (AU/d^2)	ΔT (days)	Inferred pole R.A.	Dec.	RMS
19P/Borrelly	18.2 ± 0.5	-0.6 ± 0.1	6.0 ± 0.5	-53 ± 2	205°	−5°	0.618
81P/Wild 2	15.8 ± 0.5	1.9 ± 0.3	-8.3 ± 0.4	-23 ± 6	342°	20°	0.704
2P/Encke	-0.02 ± 0.1	-0.102 ± 0.006	-9.2 ± 0.8	-1.7 ± 0.2	260°	55°	0.631
6P/d'Arrest	37.7 ± 0.6	-1.4 ± 0.3	-3.8 ± 1.0	101 ± 4	27°	−14°	0.787
67P/C.-G.	14.9 ± 0.7	-1.3 ± 0.2	5.9 ± 0.3	47 ± 4	274°	−50°	0.740
9P/Tempel 1	1.0 ± 0.3	0.06 ± 0.06	-0.4 ± 0.2	48 ± 25	N/A†		0.843

†For 9P/Tempel 1 the low significance of A_3 and ΔT indicate that a pole should not be inferred.

Table 3. Results for Rotating Jet Model

	$A_{J_1} \times 10^{10}$ (AU/d^2)	$A_{J_2} \times 10^{10}$ (AU/d^2)	η_1	η_2	Best-fit pole R.A.	Dec.	RMS
19P/Borrelly	28 ± 1	22 ± 3	10°	135°	200°	−10°	0.623
81P/Wild 2	29 ± 1	98 ± 2	8°	115°	320°	15°	0.711
2P/Encke	7.9 ± 0.4	6.5 ± 0.5	35°	165°	225°	40°	0.628
6P/d'Arrest	69 ± 4	137 ± 3	10°	135°	25°	−20°	0.779
67P/C.-G., pole A	25 ± 1	47 ± 2	10°	135°	275°	−55°	0.734
67P/C.-G., pole B	90 ± 4	47 ± 2	10°	135°	90°	75°	0.739

Note: For 9P/Tempel 1 the rotating jet model does not reveal a preferred pole orientation.

the associated optical navigation measurements were made available for improving the comet's orbit. It was only with great difficulty that these observations from the spacecraft were able to be absorbed into the fit. Even after carefully weighting and debiasing the ground-based astrometry, an acceptable fit with the two-parameter standard model (i.e., A_1 & A_2 only) still required a very short fit span, just over a single comet revolution, in order to accommodate the spacecraft observations (Chesley *et al.* 2001). The short data arc did allow us to deliver a comet ephemeris that was accurate to within about 50 km, as judged by the ground truth revealed from the successful flyby imaging. Even so, there was clearly room for improvement in modeling the Borrelly trajectory.

As a result of this experience, we extended our orbit determination software to estimate A_3 and ΔT, in addition to the conventional A_1 and A_2 parameters. We also developed, implemented and tested the rotating jet model described above. The results with the improved models were very favorable for Borrelly, as indicated by dramatically better fits and predictions.

The spacecraft encounter revealed the presence of a very strong polar jet (Soderblom *et al.* 2002) that had already been postulated by several astronomers (e.g., Farnham & Cochran 2002 and Schleicher *et al.* 2003). Because of the presence of a single dominant jet that seems to be responsible for most of the nongravitational acceleration, the values of the four ESM parameters can actually be used to orient the jet, and hence obtain a pole

https://doi.org/10.1017/S1743921304008786 Published online by Cambridge University Press

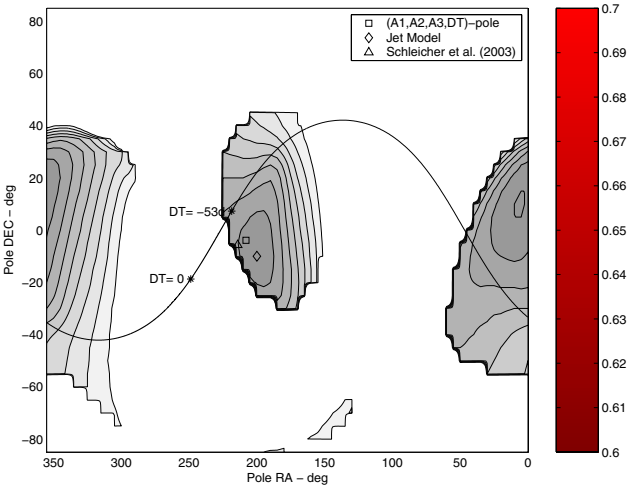

Figure 1. Contours of normalized fit RMS for 19P/Borrelly, revealing rotation poles favored by the rotating jet model. In this and subsequent plots, the blank regions of the plot correspond to nonphysical (negative thrust) jets and the solid sine wave is the locus of the comet's orbit plane. The sunward direction at $\Delta T = 0$ days (perihelion) and the best-fit $\Delta T = -53$ days (pre-perihelion) are marked. The poles derived from the RJM and ESM compare favorably with that of Schleicher *et al.* (2003) and several other published estimates (which are not plotted for the sake of clarity).

estimate. The idea is that the jet direction is given in the RTN frame by the acceleration vector (A_1, A_2, A_3) at time ΔT relative to perihelion. Simply rotating this acceleration into the equatorial frame yields the right ascension and declination of the polar jet. As indicated by Fig. 1, our pole estimate based on this method, $(\alpha, \delta) = (205°, -5°)$, compares well with the various estimates obtained by direct observation of the comet's coma.

Because Borrelly can be regarded as a ground truth for cometary jet activity and pole orientation, we use it as a test case to see whether these quantities can be inferred from the astrometry alone. To this end, we explore the entire space of possible pole orientations while assuming two jets, one at a high northern latitude of +80° and another at a mid-southern latitude of −45°. For each possible pole on a 5° grid we obtain the best-fitting jet strengths A_{J_1} and A_{J_2}. We discard as nonphysical those cases where either jet has a statistically significant negative thrust; these regions are revealed by an absence of contours in Fig. 1 and similar plots. As indicated by Fig. 1, this experiment reveals two favored pole positions. One, known *a priori* to be correct, has the northern polar jet facing sunward 50–60 days before perihelion, and the other, just slightly favored by the fits, has the 180° opposite pole so that the mid-latitude southern jet is under continuous illumination at that time. To a large extent this is merely an ambiguity in the sense of rotation; the orbit fitting is simply striving to have a maximal thrust at 50–60 days pre-perihelion, a property also replicated by the ESM. The conclusion from this test is that both models have the potential to, at least in some cases, indicate the pole orientation of a subject comet.

4.2. *Comet 81P/Wild 2*

In January 2004 the Stardust spacecraft successfully imaged Comet 81P/Wild 2 during a close flyby, producing the highest resolution images of a comet's surface obtained to

https://doi.org/10.1017/S1743921304008786 Published online by Cambridge University Press

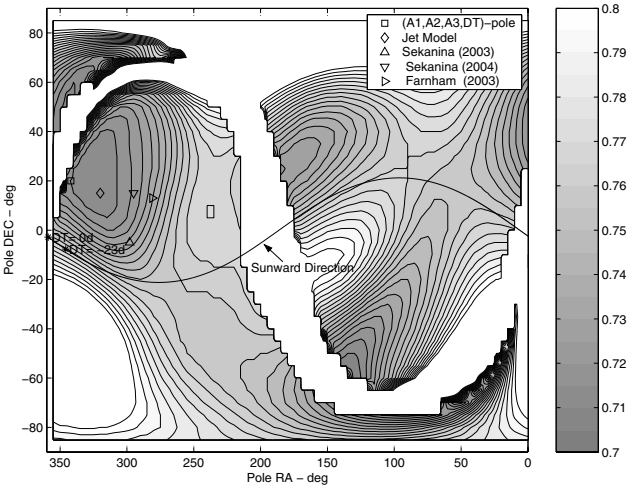

Figure 2. Contours of normalized fit RMS for 81P/Wild 2, revealing rotation poles favored by the rotating jet model. The solid sine wave defines the comet's orbit plane. The sunward direction at $\Delta T = 0$ days (perihelion) and the best-fit $\Delta T = -23$ days (pre-perihelion) are marked.

date. Sekanina *et al.* (2004) report that the flyby imaging was sufficient to reveal a spin direction around $(\alpha, \delta) = (295°, +15°)$, a result substantially consistent with earlier estimates from ground-based observations of jet activity (e.g., Farnham 2003, Sekanina 2003).

Following the RJM approach used above, we obtain the contours depicted in Fig. 2. As is clear from the figure, the poles derived from the RJM and ESM compare favorably with other published estimates obtained by direct observation. We note that Wild 2 is somewhat unusual among the comets studied so far because the 180° complement of the preferred pole positions is ruled out by the RJM. Of course, this does not reveal an independent determination of the *direction* of spin. Rather, recalling that for our tests the northen hemisphere held a near-polar jet, while the southern hemisphere had a mid-latitude jet, we conclude that the observed pre-perihelion increase in activity must be associated with a polar jet and not a mid latitude jet. Thus the seasonal effects of jetting are substantial and yield important constraints, not only on the pole position, but also on the thrust angles of the jets.

4.3. *Comet 2P/Encke*

Comet 2P/Encke was a primary target of the now-lost CONTOUR mission and was, as mentioned earlier, the first comet recognized to be affected by nongravitational accelerations. In a comprehensive study based on light curves and on the appearance of fans and jets in the morphology of Encke's coma, Sekanina (1988a, 1988b) was able to deduce two active jets, at latitudes +55° and −75°, and he was also able to infer a precession in Encke's pole direction over the years from 1868 until 1924, beyond which point Sekanina (1988b) reports that he is unable to usefully constrain the pole position with his technique.

Using his two reported jet locations (which we note are roughly symmetric with those used above for Borrelly), we find the preferred polar orientations depicted in Fig. 3. The epoch of the pole estimate given by the contours in Fig. 3 is the midpoint of the Table 1 fit span, roughly year 1997.0. This suggests that the pole has been evolving steadily along

https://doi.org/10.1017/S1743921304008786 Published online by Cambridge University Press

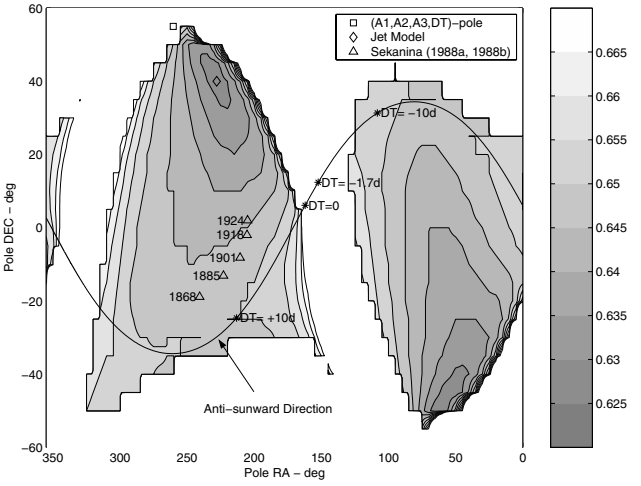

Figure 3. Contours of normalized fit RMS for 2P/Encke, revealing rotation poles favored by the rotating jet model. The solid sine wave denotes the comet's orbit plane. The anti-sunward direction at $\Delta T = 0$ days (perihelion), $\Delta T = \pm 10$ days and the best-fit $\Delta T = -1.7$ days are marked. (An anti-sunward north pole position faces Encke's south polar jet sunward.) The poles derived from the RJM and ESM suggest precession along a curved path at a more or less constant precession rate since 1868.

a roughly circular path since 1868, and fits with alternate observational arcs do indeed seem to confirm this trend. It is important to emphasize that the statistical significance of these conclusions is moderate, but not overwhelming. Even so, it is noteworthy that the inferred circular precession cycle contains the anti-perihelion vector $(\alpha, \delta) = (342°, -6°)$ near its center. Neishtadt *et al.* (2002) report that, for some comet configurations, a precession cycle centered on the perihelion direction can be a stable mode of spin state evolution, according to their modeling of discrete source outgassing.

4.4. *Comet 6P/d'Arrest*

Comet 6P/d'Arrest was a potential target for the CONTOUR mission and remains well situated for investigation by future space missions. In their original introduction of the use of ΔT, Yeomans & Chodas (1989) found this comet to have a statistically significant $\Delta T = +40$ days (with data from 1963 to 1988), in agreement with contemporaneous lightcurves. Fits of ΔT to progressively more recent data sets indicate that ΔT has been increasing steadily since about 1975, reaching a value of 101 ± 4 for the data arc considered here (Fig. 4). The most likely interpretation of this drift in DT is precession of the spin axis.

Comet 6P/d'Arrest is the first comet considered here for which we know of no independent pole information; however, we follow the approach used successfully in the three comets considered above in order to obtain a pole orientation for 6P/d'Arrest. Figure 5 indicates that the ESM-derived pole is similar to that favored by the RJM. In particular, pole positions in the region around our best-fit $(\alpha, \delta) = (25°, -25°)$ appear to be significantly favored by the RJM over those oriented in the opposite direction. This is a strong indication that the increase in post-perihelion activity is due to the action of a mid-latitude jet, rather than a near-polar jet. For this case, the right ascension of the pole is fairly well constrained, with uncertainty around $\pm 10°$, while the declination (and obliquity) are only determined to within roughly $\pm 30°$.

https://doi.org/10.1017/S1743921304008786 Published online by Cambridge University Press

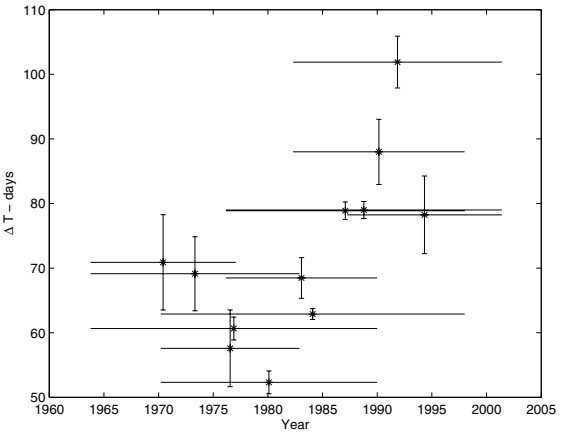

Figure 4. Best-fitting ΔT as a function of observational data set for 6P/d'Arrest with the Extended Standard Model. Horizontal lines depict the extent of observations used in fit; asterisks with error bars reflect the associated ΔT with formal uncertainty.

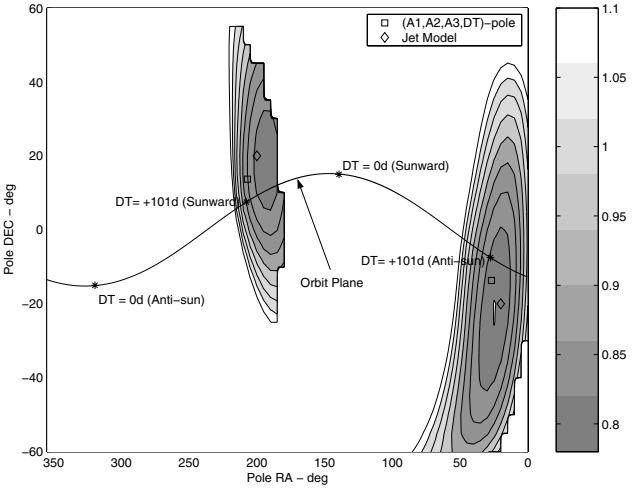

Figure 5. Contours of normalized fit RMS for 6P/d'Arrest, revealing rotation poles favored by the rotating jet model. The solid sine wave defines the comet's orbit plane. The sunward and anti-sunward directions at $\Delta T = 0$ days (perihelion) and the best-fit $\Delta T = +101$ days (post-perihelion) are marked.

4.5. *Comet 67P/Churyumov-Gerasimenko*

The recent re-targeting of the European Space Agency's Rosetta mission to 67P/Churyumov-Gerasimenko has made this comet the focus of considerable observational scrutiny. Several sources (e.g., Weiler *et al.* 2004) have reported substantially higher water and dust production rates post-perihelion, peaking 30–40 days after perihelion passage. Confirming these observations, it has been reported by Królikowska (2003) that both A_3 and ΔT are significant when using the ESM, a result with which we concur (Table 2).

We again explore the complete range of possible pole positions in the manner described earlier, and we find two favored pole orientations, which we label Pole A and Pole B. (See Table 3 and Fig. 6.) These are separated by 160°, so they are two distinct solutions,

https://doi.org/10.1017/S1743921304008786 Published online by Cambridge University Press

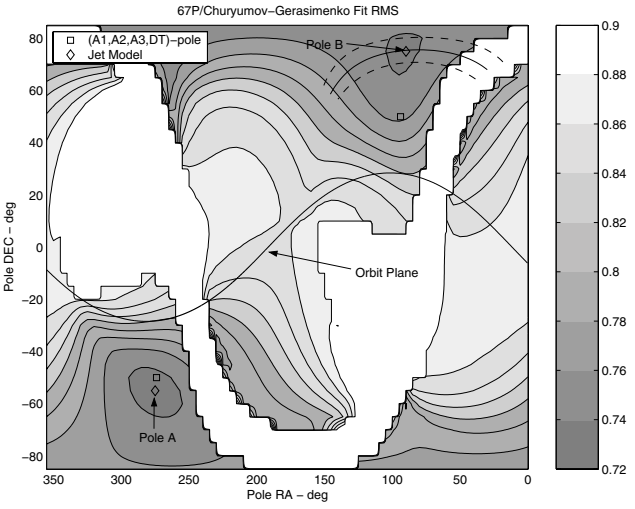

Figure 6. Contours of normalized fit RMS for 67P/Churyumov-Gerasimenko, revealing rotation poles favored by the rotating jet model. The solid sine wave defines the comet's orbit plane. The sunward and anti-sunward directions at $\Delta T = 0$ days (perihelion) and the best-fit $\Delta T = +47$ days (post-perihelion) are marked. The solid and dashed curves at upper right reflect the constraint provided by the March 2003 images of Weiler *et al.* (2004) as described in the text.

not just an ambiguity in the sense of rotation. Pole A has obliquity 117° with the north polar jet facing sunward around the time of peak outgassing. Pole B has obliquity 43° and has the mid-southern latitude jet responsible for the post-perihelion increase in activity. Statistically, there does not appear to be a substantial preference for either pole solution.

The chief distinction between the two pole solutions is whether a polar jet or a mid-latitude jet is responsible for the post-perihelion activity. Direct observational evidence strongly indicates that the latter is correct. Specifically, Weiler *et al.* (2004) report the presence of two persistent structures in images from 2003 March 7 and 28, and they suggest that these features could be the edges of a cone-shaped fan formed from a single active area on the rotating nucleus. We agree with this interpretation, and using their published images we find that the cone centerline, i.e., the projected pole, is in PA $165° \pm 5°$ and the fan extends $\pm 40°$ to either side.

In the case of a comet observed near opposition, as was the case for Churyumov-Gerasmenko in March 2003, we suppose that a rotating jet forming a cone will project as a fan-shaped structure if the pole has a modest projection angle towards the observer. If the angle is too great then the observer will be looking into the cone, which would appear more elliptical than fan-shaped; if the angle is too small, or even away from the observer (and sun), then the jet would not be sufficiently active to form a substantial cone. Thus we apply projection angles from 0° to 45° (towards the observer) to the projected PA 165 centerline and compute the associated pole positions. These are plotted in Fig. 6 as the solid curve at upper right, where the smaller projection angles appear at smaller right ascensions. The ±5° variations in PA are plotted as dashed curves.

We find it remarkable that the constraints supplied by the Weiler *et al.* images are centered on pole B, and that for projection angles around 20°—very realistic values—the two independent methods are in perfect agreement. Moreover, pole B, the pole orientation that is confirmed by the Weiler *et al.* images, is the one for which the mid-southern latitude (−45°) jet is responsible for the post-perihelion increase in activity, a point fully

https://doi.org/10.1017/S1743921304008786 Published online by Cambridge University Press

consistent with the 40° cone angle present on the March 2003 images. In contrast, if pole A were correct we would see a very narrow fan or a single collimated jet, as was the case with Borrelly. Further, in March 2003, pole A projects in PA 143°, a value incompatible with the Weiler *et al.* images.

4.6. *Comet 9P/Tempel 1*

NASA's Deep Impact mission, due to be launched in 2004 December, is planned to impact comet 9P/Tempel 1 on 2005 July 4 with a 360 kg projectile at a speed of around 10.2 km/s. The nongravitational accelerations appear to be rather unusual, being quite small and extraordinarily steady (Yeomans *et al.* 2004b). There is, for example, no difficulty in obtaining a simultaneous fit of all 8 apparitions observed since 1967. When fitting with the ESM (Table 2), only A_1 is significantly different from zero (although fixing $\Delta T = 0$ does lend substantial significance to the estimate for A_2). Also, the low significance levels for A_3 and ΔT do not allow a useful constraint to be placed on the pole orientation. While the RJM does give good fits for Tempel 1, the fit RMS is remarkably insensitive to the assumed pole position, and hence a statistically significant estimate of the pole position is not revealed. Thus, in contrast to the other five comets investigated here, neither model is capable of revealing the pole orientation of Tempel 1. All of this leads us to a few conclusions and speculations regarding Tempel 1:

- The stability of the nongravitational accelerations considerably eases the orbital prediction problem compared to other comets, making Tempel 1 an excellent target for an impacting mission such as Deep Impact.
- The low level of nongravitational acceleration implies a limited active surface area or a dwindling supply of volatiles. This line of reasoning suggests that Tempel 1 may be verging on extinction, either through depletion or some kind of mantling process.
- The nongravitational accelerations appear to have a negligible seasonal component. A possible explanation for this is that the comet's surface is more or less homogeneous so that there are not isolated active regions that account for most of the outgassing activity. Moreover, Tempel 1 has a period of about 42 hours (Belton *et al.* 2004), long enough that the diurnal thermal wave should penetrate relatively deeply, releasing volatiles that would otherwise be locked in the interior. Through this mechanism, the subsolar point may be the primary source of outgassing, effectively diminishing the signal from seasonal effects and body-fixed source regions.

5. Concluding Remarks

With these case studies we have shown that cometary spin axis information can, in many cases, be derived through measuring and modeling nongravitational accelerations on comets, although no information on the sense of rotation can be divined from these methods.

Poles inferred from the ESM assume that the nongravitational accelerations are dominated by a single high-latitude jet, a scenario that appears realistic in several of our tests, but is unlikely to be true in general. Even so, this argument suggests that a measured secular drift in ΔT should generally be interpreted as a drift in the pole orientation of the comet.

Poles obtained with the RJM are much more credible due to the more realistic nature of the modeling. Still, in the absence of corroborating measurements, such estimates should be viewed with some measure of skepticism.

We also show that the widespread assumption that comets generally have negligible out-of-plane accelerations should be revisited. In fact, we are now at a fortuitous

https://doi.org/10.1017/S1743921304008786 Published online by Cambridge University Press

point of convergence between increasing observing capabilities and improved nongravitational modeling. This suggests that a comprehensive review of the comet orbits with the techniques outlined in this paper could indicate more generally the extent to which out-of-plane accelerations are important and just how pervasive clear seasonal signals are among the comet population.

Acknowledgements

This research was conducted at the Jet Propulsion Laboratory, California Institute of Technology, under a contract with the National Aeronautics and Space Administration.

Appendix A. Rotating Jet Model

We intend to average $\mathbf{a}_J$ (Eq. 3.1) over one comet rotation. Assuming for the moment that the thrusting is symmetric about the solar meridian crossing, the averaged acceleration will be restricted to the plane containing the spin axis $\hat{\mathbf{e}}_P$ and the sun-comet line $\hat{\mathbf{r}} = \mathbf{r}/r$. This plane is defined by the normal vector

$$\hat{\mathbf{e}}_Q = \frac{\hat{\mathbf{r}} \times \hat{\mathbf{e}}_P}{|\hat{\mathbf{r}} \times \hat{\mathbf{e}}_P|} \tag{A 1}$$

The spin axis unit vector can be computed from the right ascension α and declination δ of the (assumed North) pole

$$\hat{\mathbf{e}}_P = (\cos\alpha\cos\delta,\ \sin\alpha\cos\delta,\ \sin\delta). \tag{A 2}$$

Finally, we define the $\hat{\mathbf{e}}_S$ axis

$$\hat{\mathbf{e}}_S = \hat{\mathbf{e}}_Q \times \hat{\mathbf{e}}_P, \tag{A 3}$$

which is opposite the projection of $\mathbf{r}$ on the comet's equatorial plane. This completes the right-handed (S, Q, P)-frame, in which the jet direction is given by

$$\hat{\mathbf{e}}_J = \cos\theta\sin\eta\,\hat{\mathbf{e}}_S + \sin\theta\sin\eta\,\hat{\mathbf{e}}_Q + \cos\eta\,\hat{\mathbf{e}}_P. \tag{A 4}$$

Here the rotation angle θ of the jet is measured about the pole from $\hat{\mathbf{e}}_S$ and the *thrust angle* η is the angle from $\hat{\mathbf{e}}_P$ to $\hat{\mathbf{e}}_J$. (Under the assumption that the jet is outgassing in a direction that is normal to the surface of a spherical comet, η is the colatitude of the jet's location.)

The insolation term $(\cos z)$ of Eq. 3.1 can be cast in terms of the rotation angle θ and the thrust angle η according to

$$\cos z = \cos\eta\cos\gamma + \sin\eta\sin\gamma\cos\theta, \tag{A 5}$$

where $\cos\gamma = -\hat{\mathbf{r}} \cdot \hat{\mathbf{e}}_P$, γ being the colatitude of the subsolar point.

The jet is on the terminator when $\cos z = 0$, that is, when

$$\cos\theta^* = -\frac{\cos\eta\cos\gamma}{\sin\eta\sin\gamma}, \tag{A 6}$$

where $\theta^* > 0$ is the rotation angle that places the jet on the afternoon terminator. If $\cos\theta^* < -1$ then the sun is never below the horizon and we explicitly define $\theta^* \doteq \pi$. Similarly, if $\cos\theta^* > 1$ then the sun is never above the horizon and $\theta^* \doteq 0$. These situations represent, respectively, the polar day and polar night regimes. Intermediate values of $\cos\theta^*$ correspond to the day-night, or diurnal, regime. In each of these three regimes the jet is illuminated over the interval $-\theta^* < \theta < \theta^*$, and this is the interval across which we wish to integrate Eq. 3.1 when averaging, since elsewhere the acceleration is zero.

Combining Eqs. 3.1 and A 4, we recast the instantaneous acceleration as

$$\mathbf{a}_J = -A_J\, g(r)\, \cos z\, (\cos\theta \sin\eta\, \hat{\mathbf{e}}_S + \sin\theta \sin\eta\, \hat{\mathbf{e}}_Q + \cos\eta\, \hat{\mathbf{e}}_P) \tag{A 7}$$

and average over one rotation according to

$$\bar{\mathbf{a}}_J = \frac{1}{2\pi} \int_{-\theta^*}^{\theta^*} \mathbf{a}_J\, d\theta = A_J\, g(r)\, \mathbf{J}, \tag{A 8}$$

where

$$\mathbf{J} = J_S\, \hat{\mathbf{e}}_S + J_P\, \hat{\mathbf{e}}_P. \tag{A 9}$$

The terms J_S and J_P are zero for the polar night regime ($\theta^* = 0$) and take on simple forms for the polar day regime ($\theta^* = \pi$)

$$J_S = -\frac{1}{2} \sin^2\eta \sin\gamma, \quad J_P = -\cos^2\eta \cos\gamma. \tag{A 10}$$

For the diurnal regime, we use Eq. A 5 to compute these terms

$$\begin{aligned} J_S &= -\frac{\sin\eta}{2\pi} \int_{-\theta^*}^{\theta^*} \cos z \cos\theta\, d\theta \\ &= -\frac{\sin\eta}{\pi} \left[\cos\eta \cos\gamma \sin\theta^* + \frac{1}{2} \sin\eta \sin\gamma\, (\theta^* + \cos\theta^* \sin\theta^*) \right] \\ J_P &= -\frac{\cos\eta}{2\pi} \int_{-\theta^*}^{\theta^*} \cos z\, d\theta = -\frac{\cos\eta}{\pi}\, (\theta^* \cos\eta \cos\gamma + \sin\eta \sin\gamma \sin\theta^*)\,. \end{aligned} \tag{A 11}$$

Note that the Q-component of acceleration has been eliminated by the averaging process because of the assumption that outgassing peaks at the solar meridian crossing and that the outgassing profile is symmetric about this point. However, if the diurnal acceleration peak actually occurs at a point other than $\theta = 0$, which may be expected if, for example, surface thermal inertia causes a diurnal lag, then there will be some component of acceleration in the $\hat{\mathbf{e}}_Q$ direction. To model this possibility we simply rotate $\hat{\mathbf{e}}_S$ by a diurnal lag angle $\Delta\theta$ to obtain a new equatorial direction for the averaged acceleration

$$\hat{\mathbf{e}}_E = \cos\Delta\theta\, \hat{\mathbf{e}}_S + \sin\Delta\theta\, \hat{\mathbf{e}}_Q, \tag{A 12}$$

so that, with a non-zero diurnal lag $\Delta\theta$,

$$\mathbf{J} = J_S\, \cos\Delta\theta\, \hat{\mathbf{e}}_S + J_S\, \sin\Delta\theta\, \hat{\mathbf{e}}_Q + J_P\, \hat{\mathbf{e}}_P. \tag{A 13}$$

If $\hat{\mathbf{e}}_P$ represents the North pole then one should expect $\Delta\theta > 0$ due to thermal inertia. On the other hand, $\Delta\theta < 0$ would suggest that $\hat{\mathbf{e}}_P$ is actually the South pole.

Of course, we can have more than one jet acting on the comet, in which case we can simply sum the contributions from each, using the subscript i to distinguish the contributions of the various jets:

$$\bar{\mathbf{a}}_J = g(r) \sum_{i=1}^{n} A_{J_i}\, \mathbf{J}_i. \tag{A 14}$$

The partial derivatives of the acceleration with respect to $\mathbf{r}$, $\mathbf{v}$ and any estimable model parameters are required as a part of the orbit determination process. The basic equations for these derivatives are

$$\frac{\partial \bar{\mathbf{a}}_J}{\partial \mathbf{r}} = \frac{\partial g(r)}{\partial \mathbf{r}} \sum_{i=1}^{n} A_{J_i} \mathbf{J}_i + g(r) \sum_{i=1}^{n} A_{J_i} \frac{\partial \mathbf{J}_i}{\partial \mathbf{r}}$$

https://doi.org/10.1017/S1743921304008786 Published online by Cambridge University Press

$$\frac{\partial \bar{\mathbf{a}}_J}{\partial A_{J_i}} = g(r)\mathbf{J}_i; \quad \frac{\partial \bar{\mathbf{a}}_J}{\partial(\alpha,\delta)} = g(r)\sum_{i=1}^{n} A_{J_i}\frac{\partial \mathbf{J}_i}{\partial(\alpha,\delta)}$$

$$\frac{\partial \bar{\mathbf{a}}_J}{\partial \eta_i} = g(r)A_{J_i}\frac{\partial \mathbf{J}_i}{\partial \eta_i} = g(r)A_{J_i}\left(\frac{\partial J_{S_i}}{\partial \eta_i}\hat{\mathbf{e}}_E + \frac{\partial J_{P_i}}{\partial \eta_i}\hat{\mathbf{e}}_P\right)$$

$$\frac{\partial \bar{\mathbf{a}}_J}{\partial \Delta\theta} = g(r)\sum_{i=1}^{n} A_{J_i}\frac{\partial \mathbf{J}_i}{\partial \Delta\theta} = g(r)\,(-\sin\Delta\theta\,\hat{\mathbf{e}}_S + \cos\Delta\theta\,\hat{\mathbf{e}}_Q)\sum_{i=1}^{n} A_{J_i}J_{S_i}$$

The derivatives $\partial \mathbf{J}_i/\partial \mathbf{r}$ and $\partial \mathbf{J}_i/\partial(\alpha,\delta)$ are fairly complex and we compute these through finite differences. Other terms can be computed analytically.

References

Belton, M.J.S., Meech, K.J., A'Hearn, M.F. & 10 coworkers 2004, *Space Sci. Rev.*, in press

Bessel, F.W. 1836, *Astron. Nach.* 13, 345

Chesley, S.R. 2002, *Bull. Am. Astr. Soc.* 34, 869

Chesley, S.R., Chodas, P.W., Keesey, M.S., Bhaskaran, S., Owen, W.M., Jr., Yeomans, D.K., Garradd, G.J., Monet, A.K.B. & Stone, R.C. 2001, *Bull. Am. Astr. Soc.* 33, 1116

Encke, J.F. 1823, in: *Berliner Astronomische jahrbuch fur das jahr 1826* (Berlin) p. 124

Farnham, T.L. 2003, *Bull. Am. Astr. Soc.* 35, 971

Farnham, T.L. & Cochran, A.L. 2002, *Icarus*, 160, 398

Kamieński, M. 1933, *Acta Astron., Series A* 3, 1

Królikowska, M. 2003, *Acta Astron.* 53, 195

Królikowska, M., Sitarski, G. & Szutowicz, S. 1998, *Astron. Astrophys.* 335, 757

Marsden, B.G., Sekanina, Z. & Yeomans, D.K. 1973, *Astron. J.* 78, 211

Neishtadt, A.I., Scheeres, D.J., Sidorenko, V.V. & Vasiliev, A.A. 2002, *Icarus* 157, 205

Recht, A.W. 1940, *Astron. J.* 48, 65

Schleicher, D.G., Woodney, L.M. & Millis, R.L. 2003, *Icarus* 162, 415

Sekanina, Z. 1981, *Annual Rev. Earth Planet. Sci.* 9, 113

Sekanina, Z. 1984, *Astron. J.* 89, 1573

Sekanina, Z. 1988a, *Astron. J.* 95, 911

Sekanina, Z. 1988b, *Astron. J.* 95, 1455

Sekanina, Z. 1993, *Astron. J.* 105, 702

Sekanina, Z. 2003, *J. Geophys. Research* 108, 8112

Sekanina, Z., Brownlee, D.E., Economou, T.E., Tuzzolino, A.J. & Green, S.F. 2004, *Science* 304, 1769

Sitarski, G. 1995, *Acta Astron.* 45, 763

Sitarski, G. 1996, *Acta Astron.* 46, 29

Soderblom, L.A., Becker, T.L., Bennett, G. & 19 coworkers 2002, *Science* 296, 1087

Szutowicz, S. 2000, *Astron. Astrophys.* 363, 323

Weiler, M., Rauer, H., Helbert, J. 2004, *Astron. Astrophys.* 414, 749

Whipple, F.L. 1950, *Astron. J.* 111, 375

Whipple, F.L. 1951, *Astrophys. J.* 113, 464

Whipple, F.L. & Sekanina, Z. 1979, *Astron. J.* 84, 1894

Yeomans, D.K. & Chodas, P.W. 1989, *Astron. J.* 98, 1083

Yeomans, D.K., Chodas, P.W., Sitarski, G., Szutowicz, S. & Królikowska, M. 2004a, in: M. Festou (ed.), *Comets II* (Univ. Arizona), in press

Yeomans, D.K., Giorgini, J.D. & Chesley, S.R. 2004b, *Space Sci. Rev.*, in press